

Human Preference Modeling Using Visual Motion Prediction Improves Robot Skill Learning from Egocentric Human Video

Mrinal Verghese

Robotics Institute Carnegie Mellon University
Email: mverghes@andrew.cmu.edu

Christopher G Atkeson

Robotics Institute Carnegie Mellon University
Email: cga@andrew.cmu.edu

Abstract—We present an approach to robot learning from egocentric human videos by modeling human preferences in a reward function and optimizing robot behavior to maximize this reward. Prior work on reward learning from human videos attempts to measure the long-term value of a visual state as the temporal distance between it and the terminal state in a demonstration video. These approaches make assumptions that limit performance when learning from video. They must also transfer the learned value function across the embodiment and environment gap. Our method models human preferences by learning to predict the motion of tracked points between subsequent images and defines a reward function as the agreement between predicted and observed object motion in a robot’s behavior at each step. We then use a modified Soft Actor Critic (SAC) algorithm initialized with 10 on-robot demonstrations to estimate a value function from this reward and optimize a policy that maximizes this value function, all on the robot. Our approach is capable of learning on a real robot, and we show that policies learned with our reward model match or outperform prior work across multiple tasks in both simulation and on the real robot.

I. INTRODUCTION

How can we dramatically reduce the number of on-robot demonstrations needed to learn basic skills by transferring information from human video demonstrations of skills to robots learning these same skills? When training robots with teleoperation demonstrations collected on the robot, there often exists a “skill-gap” where the learned policy underperforms the demonstrations. This gap exists because robot teleoperation demonstrations are expensive to collect and often only cover a portion of the task space. Videos of humans performing household tasks are a readily available source of supervision. These videos can help close this gap by covering more of the task space, but robots face challenges in learning from this data due to mismatches in the actor embodiment and the environment. A very promising approach to leverage human video for robot skill learning is to learn a feedback signal, such as a reward or cost function, from large video datasets, and then optimize this function on the robot via planning or reinforcement learning. This approach helps mitigate the embodiment gap and does not require tracking and imitating human hand or object trajectories, methods that can struggle with contact-rich tasks or require large amounts of on-robot data. The most common strategy to learn these feedback signals is to estimate the long-term value $V(s)$ of a state as its temporal distance to the goal (the last frame in a video demonstration) by assuming every frame in the demonstration incurs

a fixed per-frame cost and assigning the value of a visual state as its frame distance to the goal [30, 34, 33, 50, 39]. However, this strategy is susceptible to noise in the demonstration data and can have trouble generalizing this learned value function to robot videos and recognizing failed attempts. In this work, we present a novel method of learning reward functions from large human video datasets and argue that representing human preferences via visual motion features is a more effective way to learn a reward function from human video demonstrations.

There are several challenges associated with learning robot reward signals from large, unstructured human video datasets. These datasets generally only contain successful demonstrations, and methods that do not select the right features to attend to may falsely reward episodes that look similar to the demonstrations but do not achieve the same effect. Humans often multitask, and video datasets contain many instances where a human may interrupt one skill to perform another, hesitate during a skill, or otherwise not act in a time-optimal manner. Methods that measure value by temporal distance to the goal will negatively bias all states before any such interruption. Finally, there is a large distribution shift between human video and robot video, and whatever quantity that is learned from human video must be transferred across this gap in a robust way.

In this work, we approach reward learning as a problem of modeling the short-term preferences of human demonstrators at each step in a demonstration. We learn models to predict how tracked points on task-relevant objects in a demonstration video move at each step, and assign a per-transition reward to a robot rollout based on the alignment between the predicted point motion and the observed point motion induced by the robot’s actions. We then utilize a modified version of the Soft Actor Critic (SAC) algorithm to estimate the long-term value of a state in the robot’s state distribution and optimize a policy to maximize this value. By predicting point motion of task-relevant objects, and rewarding the robot for matching this point motion, we explicitly encourage the robot to match the outcomes of the human demonstrations and not just the human’s actions. By modeling short-term preferences rather than long-term value estimates, our approach is less susceptible to bias from hesitation or distractions in the demonstrations or from distribution shift.

To improve a behavior-cloned robot policy’s performance on a specific task, our method first analyzes a set of ego-

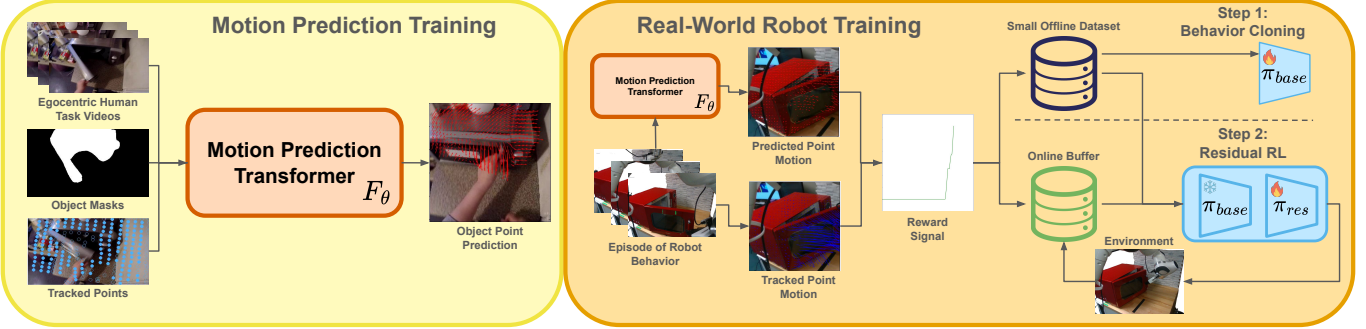


Fig. 1: Modeling human preferences using Motion Prediction Reward improves robot skill learning from human video data. To learn a robust reward signal from human video for a given task \mathcal{T} (in this case, “Open Microwave”), we first extract point tracks and object masks using off-the-shelf models from a set of egocentric human videos demonstrating \mathcal{T} . This data is used to train our Motion Prediction Transformer (F_θ) that can predict how points on an object will move given a visual observation. This model is used to calculate reward for an episode of robot behavior, by tracking points in a video of the episode, and measuring the alignment between predicted and observed point motion at each transition. To learn a robot policy for task \mathcal{T} , we collect a very small set of demonstrations (small offline dataset) and train a behavior cloning policy (π_{base}) to kickstart learning. We then use a sample-efficient residual RL framework that leverages both the collected demonstrations and new episodes from online interaction (online buffer), labeled with our reward model, to improve its performance on the given task. This process is able to increase a robot’s success rate on a task by over 30% with just an hour of real-world interaction, and significantly outperforms prior work on reward learning from human video.

centric videos of humans performing that task, and outputs a preference model that predicts how a set of tracked points across task-relevant objects will move between frames. For each attempt the robot makes to complete the task, we compare the predicted point motion at each transition with the observed point motion to generate a reward signal. We then use an actor-critic reinforcement learning algorithm in a residual RL framework that learns a value function and policy corrections on top of the behavior-cloned policy to make the robot’s behavior more closely match the predicted human preferences. This pipeline is highlighted in Figure 1. This RL framework combines modern advances in imitation learning, such as diffusion policies, with sample-efficient reinforcement learning techniques to enable practical online finetuning of robot policies in the real world. We demonstrate the performance of this approach in a real-world reinforcement learning setting across three tasks using our learned reward models, and show that our method can enable a robot to rapidly improve its own performance in only an hour of wall-clock training time.

II. RELATED WORKS

A. Robot Learning with Human Video Data

Human video data exists in large quantities on the internet, is easy to collect, and has the potential to greatly reduce the number of on-robot demonstrations needed to learn new robot skills. To accomplish this, prior work has explored a wide variety of approaches to transfer information from this data source to robot policies. Several works have explored objectives like contrastive learning [41] and masked autoencoding [36] to learn general-purpose visual encoders from common egocentric video datasets such as Ego4D [15] and Epic Kitchens [12, 13]. These vision encoders have primarily been used to reduce the visual learning burden when learning robot policies, but are also capable of measuring similarity between states to determine reward. Recently, the popular

Vision-Language-Action (VLA) architecture has been adapted to use video generation models trained on human videos as their pretrained backbone [52, 25]. These Video VLA models show promising improvements over existing VLAs, but also suffer from some of the drawbacks of VLAs, including being expensive to train and finetune. Other works have trained world models using human video data that are capable of forecasting actions into the future [25, 4, 54]. Finally, a large body of work has examined directly translating human videos into robot behavior. The approaches can be broken down into three main categories. The first category attempts to directly mimic or forecast the trajectory of objects in a video and then solve for a set of robot actions to match that object trajectory in the real world [19, 43, 8, 28]. Some of these methods can learn from a single video demonstration, but as they compute trajectories and not closed-loop policies, they tend to be less robust and struggle with contact-rich tasks. Several of these works do collect extra robot data to mitigate this limitation [8, 28]. The next category is methods that perform imitation learning on human videos by tracking human hands and retargeting the human hand actions to a robot’s action space [45, 5, 24, 29, 48, 27]. These methods show impressive generalization, but depend heavily on how the human-to-robot retargeting is done and usually require either in-domain videos (as opposed to internet videos) in the target environment or reasonable amounts of robot data. Finally, recent work by Yuan et al. [56] shows impressive real-world results by leveraging reinforcement learning to better track trajectories from videos. However, this approach requires recreating both the robot and environment in simulation and transferring the policy learned in simulation back to the real world. This requires significant engineering effort and can be challenging for tasks involving deformable objects.

B. Learning Visual Reward Models in Robotics

In this work, we address the problem of learning reward models that operate on visual inputs. Estimating rewards from visual input enables reward learning from diverse sources, including pretrained image [35] and video [51] models, diverse robot datasets [26], robot video [30, 14, 37], in-domain human video demonstrations [30, 50, 18], and large video datasets [39, 34, 33]. Most of these approaches learn an encoder that maps visual state into a latent space, and measures the distance between a visual observation and a goal input in that latent space to determine the value of a visual state. For the visual reward learning methods that leverage video demonstrations, they primarily train these encoders to estimate the temporal distance between a visual state and a goal, as measured by the number of frames between them [30, 34, 33, 50, 39]. While this metric is convenient for video data and has demonstrated success in the past, it can be less effective for training on large-scale video datasets due to the issues highlighted above. We compare our approach to VIP from Ma et al. [34] due to its similar training data (large-scale egocentric human video datasets), and available pretrained models. It's important to note that our reward model can easily be composed with other learned reward signals. A practical deployment of reward models for robot learning might combine an approach like ours that provides dense, per-step feedback, with an approach like RoboReward from Lee et al. [26] that provides a high-level success indication at the end of an episode. Finally, there is also a large body of work in Inverse Reinforcement Learning, which learns reward functions from expert demonstrations on the robot, but this work often operates under a very different set of assumptions from visual reward learning.

C. Robot Learning from Demonstration and Practice

To enable our robot to improve its performance with our reward signal, we turn to the field of learning from demonstration and practice. Reinforcement Learning (RL) is a powerful method for optimizing robot behavior according to a reward or cost function, but it is also notoriously sample inefficient, particularly in its initial exploration phase. Combining RL with a small set of on-robot demonstrations helps shortcut this sample inefficient exploration phase and greatly accelerates the learning process. Some prior work in this area used parameterized primitives to simplify the action space and enable efficient online adaptation [7, 55]. A large body of recent work has explored adapting behavior cloned neural network policies with reinforcement learning on real robot hardware [2, 3, 31, 32, 21, 20, 38, 6, 47]. The primary challenge in this area is to make an algorithm that is both stable and sample-efficient. Some works have tackled this by identifying design decisions to make existing Off-Policy RL algorithms like Soft Actor Critic (SAC) [17] work nicely for real-world learning [6, 31, 32]. Other works have eschewed typical RL training objectives like policy gradients or Q-function maximization for supervised learning, which is typically more stable [21, 38]. Finally, a set of work has looked at residual RL, where a base behavior cloned policy is kept frozen during training, and RL learns a residual policy

on top to apply corrections to the base policy [2, 3]. This work has been able to leverage powerful behavior cloning architectures like diffusion policies [10] for the frozen base policy, which other work has shown can be challenging to finetune directly [47]. We draw insights from RLPD (Ball et al. [6]), SERL (Luo et al. [31]), ResiP (Ankile et al. [2]) and ResFit (Ankile et al. [3]) when designing our Off-Policy Residual RL framework.

III. METHODS

In our problem setting, we are given a large set of human video demonstrations $\mathcal{V} = \{\langle o_0, o_1, \dots, o_T \rangle \dots\}$ and a small set of on-robot demonstrations $\mathcal{D} = \{\langle (s_0, a_0), (s_1, a_1), \dots, (s_n, a_n) \rangle \dots\}$ on a task \mathcal{T} specified via a language tag. A policy π trained only on \mathcal{D} is not sufficiently performant on task \mathcal{T} , so we seek to derive a reward signal $R(s, a)$ such that if we adapted π to maximize the value function $V(s_t) = E\left[\sum_{t=0}^{\infty} \gamma^t R(s_t, \pi(s_t))\right]$ computed with this reward, π would increase its performance on task \mathcal{T} . This problem is particularly challenging as not only does the agent in \mathcal{V} have a different action space from our robot, but we also cannot directly observe actions in \mathcal{V} , only the visual changes resulting from these actions. Note that we make a distinction between states (s_t) and observations (o_t), where states contain visual information from static cameras and robot-mounted cameras and proprioceptive information from the robot, while observations contain only a single camera observation. Observations can be extracted from both human videos \mathcal{V} and robot data \mathcal{D} while states are only available in robot data \mathcal{D} .

Our approach learns a motion prediction model $P_{t+1} = F_{\theta}(o_t, P_t, t/T)$ from \mathcal{V} where o_t is a visual observation at time t , P_t is the locations of a set of points, and t/T is a normalized task progress indicator. This model F_{θ} captures the “preferences” of the human demonstrators at each step in the task. For each attempt the robot makes at task \mathcal{T} , we measure the agreement between the predicted and observed motion between frames as our reward signal. Finally, an actor-critic algorithm uses this signal to estimate a value function and learn corrections to π that increase its performance on task \mathcal{T} .

A. Reward Learning as Modeling Expert Preferences

The first stage of our approach is training our motion prediction model F_{θ} using human data \mathcal{V} . We first preprocess the data by tracking masks of task-relevant objects through each video, as well as tracking a grid of sampled points across the video. F_{θ} is then trained to output the location of a set of points at time $t+1$ given their locations at time t as well as an observation from time t . To compute a reward signal for an episode of robot behavior, we extract observations $\langle o_0, o_1, \dots, o_T \rangle$, detect and track masks for task-relevant objects, and track a set of points $\langle P_0^{track}, P_1^{track}, \dots, P_T^{track} \rangle$ across the episode. Using these observations, point locations, and F_{θ} , we compute a set of predicted point locations for each step in the episode $\langle P_1^{pred}, P_2^{pred}, \dots, P_T^{pred} \rangle$. For each point $p \in P$, we compute a vector for how we predicted it to move between frames t and $t+1$, $\Delta p_t^{pred} = p_{t+1}^{pred} - p_t^{pred}$, and how it was observed

to move between frames $\Delta p_t^{track} = p_{t+1}^{track} - p_t^{track}$. With this information, we can compute the reward signal for frame t as:

$$r_t = \sum_{\substack{\Delta p_t^{pred} \in \Delta P_t^{pred}, \\ \Delta p_t^{track} \in \Delta P_t^{track}}} \max \left(\frac{\Delta p_t^{pred} \cdot \Delta p_t^{track}}{\|\Delta p_t^{pred}\| \|\Delta p_t^{track}\|}, 0 \right) \quad (1)$$

where ΔP_t^{pred} and ΔP_t^{track} are the set of predicted and tracked point deltas, respectively, at time t . Essentially, this reward computation is measuring the alignment (positive cosine similarity) between predicted and tracked point deltas at each time step. If we consider the predicted point deltas to capture the one-step preferences of the human demonstrator, i.e., how objects tend to move at each step in the task, then this reward signal rewards the robot for taking actions that match these preferences. See section VII in the appendix for further details on this implementation.

This approach has several advantages over prior work that measures the value of a visual state as its temporal distance to the goal. Prior work defines a value function as $V(o_t) = \sum_t^T -1$ for each demonstration video, where observations with further temporal distance from the goal have lower value and learn a model $V_\phi(o_t)$ to predict this value function conditioned on o_t . As mentioned, hesitations or non-time-optimal actions by the human demonstrator at time t will negatively bias the value of all prior observations $\langle o_0, o_1, \dots, o_{t-1} \rangle$. By measuring reward r_t conditioned only on prediction and track deltas ΔP_t^{pred} and ΔP_t^{track} at time t , only the reward estimate at time t is biased. $V_\phi(o_t)$, which is trained on only human video data, must also transfer its value estimates to videos of robots performing tasks, a significant distribution shift that may incur unexpected biases in predicted value. By only computing reward using point deltas on task-relevant objects, we lessen the distribution shift in jumping the embodiment gap from humans to robots and focus on the features that are consistent between these two domains. In addition, computing reward only across task-relevant objects incentivizes the robot to match the outcomes of human actions, not the actions themselves. This quality helps distinguish unsuccessful attempts that have approximately the right motions from genuinely successful attempts.

While our method predicts single step reward, instead of estimating long-term value like prior work, practically, this is a non-issue. Any modern reinforcement learning framework will first learn a value function as $Q_\psi(s_t, a_t) = R(s_t, a_t) + \gamma Q_\psi(s_{t+1}, \pi(s_{t+1}))$ before performing any policy gradient or actor loss calculation, and this value function is likely to be more accurate as it is computed on the robot state distribution, and not the human video observation distribution.

Finally, readers familiar with the no-regret learning literature may observe similarities between our approach and DAgger [49]. Given an expert policy, DAgger trains a learner policy to match the expert's action in every state the learner visits. Ross et al. [49] observe that a learner that matches the expert's preferences on the learner's state distribution is more likely to converge to a good policy than a learner who trains to match the expert's preferences on the expert's state distribution, as in typical behavior cloning. A robot that

optimizes a policy to maximize the reward function computed with our approach is learning to match the estimated expert preferences in its own state distribution.

B. Point Prediction Model

In this work, we use visual point tracks in a video as a representation of preferences for robot learning. Point tracking models take in a set of frames $\langle o_0, o_1, \dots, o_T \rangle$ where $o_t \in \mathbb{R}^{H \times W \times 3}$ and a set of query points $\mathcal{P} = [p_1, p_2, \dots, p_k]$ with $p_i = (x_t, y_t) \in \mathbb{R}^2$ where (x_t, y_t) is the query point location at frame t . These models then output the image location of each point p_i across the entire video $(x_t, y_t)_{t=1}^T$. Recent advances in point tracking models, such as CoTracker3 [23, 22], show remarkably robust performance across many “in-the-wild” videos, leading us to choose this representation for our work.

Our motion prediction model $F_\theta(o_t, P_t, \tau) = P_{t+1}$ parameterized by weights θ takes in an observation o_t a set of query points P_t and a normalized task time scalar $\tau = t/T$ and outputs the locations of the query points in the next frame P_{t+1} . For a video $\langle o_0, o_1, \dots, o_T \rangle$ with tracked points $\langle P_0^{track}, P_1^{track}, \dots, P_T^{track} \rangle$ we train F_θ with a simple regression loss:

$$l(\theta) = \|F_\theta(o_t, P_t, t/T) - P_{t+1}\|^2 \quad (2)$$

We model F_θ with a modified version of the DiT architecture from the Diffusion Transformer paper [44]. While we train our model with regression, not diffusion, we find the DiT architecture is useful to model how a set of input points changes given various conditioning features. While the standard DiT architecture conditions the main body of the transformer with feature-wise linear modification (FiLM), and previous work by Bharadhwaj et al. [8] that predicted point motion with this architecture used a ResNet encoder with a single vector output to condition the model, we add a cross-attention layer with visual tokens from a frozen DinoV2 [42] pretrained vision transformer. We find that DinoV2 provides robust visual features that reduce the learning burden on our model, and the spatial information from visual tokens improves the prediction of point motion. This training is visualized in the yellow portion of figure 1. Further training details can be found in Appendix section VII.

C. Egocentric Human Video Preprocessing

To learn from noisy and unstructured human video, our pipeline includes important preprocessing steps to extract the relevant inputs to our point prediction model F_θ from the human video dataset \mathcal{V} . For a task \mathcal{T} specified by a language tag, we first retrieve a set of videos with labels matching \mathcal{T} from the Ego4D [15] and Epic Kitchens [13] datasets. While in this work, we retrieve based on matching language tags, we also saw success with using embeddings computed by the LaViLa model [57], which would enable this work to scale to unlabeled videos. We use a combination of an open-vocabulary object detection model, OWLViT2 [40], a segmentation model, SAM2 [46], and a mask tracker, Cutie [9] to detect, segment, and track task-relevant objects. As the clip start and end times in large online video datasets are not always completely accurate, we trim portions of the video where task-relevant objects are not visible. We then track a grid of points through

the video and, using the tracked object masks, separate these points into a set of object points and background points. To compensate for the significant camera motion in egocentric video, we subtract the mean of the background point motion between frames from both the object point deltas and the background point deltas. Finally, we train the model with a weighted mixture of object and background points. Further details on data preprocessing are available in section VII.

D. Residual Reinforcement Learning

To optimize a policy π to maximize our reward function, we leverage methods in the learning from demonstration and practice literature. To create a learning pipeline that is both sample-efficient and stable, we combine insights from several prior works. Work by Ankile et al. [2] trains a diffusion policy[47] on a set of demonstration data and then learns a residual policy with reinforcement learning that applies corrective actions Δa to improve the performance of the base policy. Importantly, the base policy is frozen during this training, and only the residual corrective action is learned. While the original work used PPO, we found in experiments that if the residual policy ever pushed the robot too far outside the distribution of the demonstration data \mathcal{D} , the policy learning would usually collapse. To remedy this, we draw insights from work by [6], which identifies a set of design decisions to enable off-policy RL algorithms such as Soft Actor-Critic (SAC) [17] to effectively leverage an offline dataset \mathcal{D} along with an online buffer \mathcal{B} of data collected from the robot interacting with the environment during training. Specifically, they take the minimum value across multiple critic networks and use LayerNorm in these critic networks to reduce the likelihood that the critic function overestimates value in low-data regions of task space. This decision reduces the likelihood of the actor falsely exploiting value overestimates. They also sample equally from \mathcal{D} and \mathcal{B} during training. We implement these two modifications, as well as pretraining the critic on offline data \mathcal{D} labeled with rewards from our reward function to warm-start online finetuning. Importantly, for a given state-action pair (s_t, a_t) in the offline data \mathcal{D} , we replace a_t with Δa_t by subtracting the output of the base policy from a_t . Our combined policy executed during online training is given by $\pi(s) = \pi_{base}(s) + \alpha \pi_{RL}(s)$ where π_{base} is the frozen base policy learned with behavior cloning, π_{RL} is the residual reinforcement policy, and alpha is a scalar constant that limits the magnitude of the residual actions. We find that even when using a base policy, training with the offline dataset \mathcal{D} serves as a regularizer to prevent the actor from straying too far away from the demonstration data (as the residual actions for states in the demonstration data are close to 0). While freezing the base policy and applying a regularizer to ensure the learned policy does not deviate significantly from the data distribution of the base policy can potentially limit performance, we find that the stability improvements are well worth it, especially in a real-world finetuning scenario. Some of these design decisions also appear in work by Luo et al. [31] and concurrent work by Ankile et al. [3]. Overall, our experimentation here reaffirms what many others working in RL have found; regularization, both in learned value functions to prevent overestimation and in policies to prevent the policy from straying too far from regions of good data, is crucial

to building stable and efficient RL pipelines. This training is visualized in the rightmost portion of figure 1. Further details about our residual RL implementation can be found in Appendix section VIII.

IV. RESULTS

A. Simulation Results

We first evaluate the performance of our approach on two tasks, “Open Microwave” and “Open Cabinet”, in the simulated Franka Kitchen [16] benchmark. We chose these two tasks as they are well represented in the Ego4D [15] and Epic Kitchens [13] egocentric video datasets from where we retrieve human video demonstrations. We compare our approach to several baselines. The first is a sparse reward function, which gives 1 on task success and 0 otherwise. Second, we compare with a hand-designed dense reward function that uses privileged state information (the positions and angles of relevant objects) in its reward computation. Finally, we compare with Value Implicit Pretraining (VIP) [34], a representative approach from the class of temporal-distance-based value functions learning methods that we select for its easily available models and similar training data. We refer to our approach as Motion Prediction Reward (MPR) for experiments.

Each model uses a frozen base policy trained on 20 demonstrations from the simulated benchmark, and these demonstrations are also added to the offline data buffer \mathcal{D} . The models are trained for 300,000 simulated steps and evaluated every 50,000 steps for 20 episodes. The values plotted are the mean and standard deviations (shaded portions) of success rates across 8 seeds for each method. We plot the performance of the best checkpoint so far at each evaluation step. Note the methods initially underperform the base policy due to the randomly initialized residual policy which adds noise to the base policy actions. All training parameters can be found in the Appendix in section X

As shown in Figure 2, while MPR, VIP, and the handcrafted dense reward function all perform similarly on the “Open Cabinet” task, MPR clearly outperforms VIP in the “Open Microwave” task and closely tracks the performance of the handcrafted dense reward function. Examining the estimated reward signals across 50 successful demos for the “Open Microwave” in Figure 3 task illustrates why. While our reward signal very closely tracks the handcrafted reward signal, VIP shows biases in the reward signal for certain states, which lead a learning agent into local minima and slow learning.

B. Hardware Experiments

To validate our reward learning approach on real robot hardware, we test it across three tasks. In “Open Microwave”, the robot must grasp the handle of a microwave to pull the door open. In “Fold Cloth”, the robot must fold a square cloth corner-to-corner into a triangle. And finally, in “Wipe Counter,” a robot must pick up a folded towel and use it to wipe coffee grounds off the counter into a bin. We use a Franka Research 3 equipped with UMI [11] fingers and two Realsense D435 cameras, one looking over the robot’s shoulder, called the world camera, and one mounted just above the robot’s gripper, called the wrist camera. All observations for reward

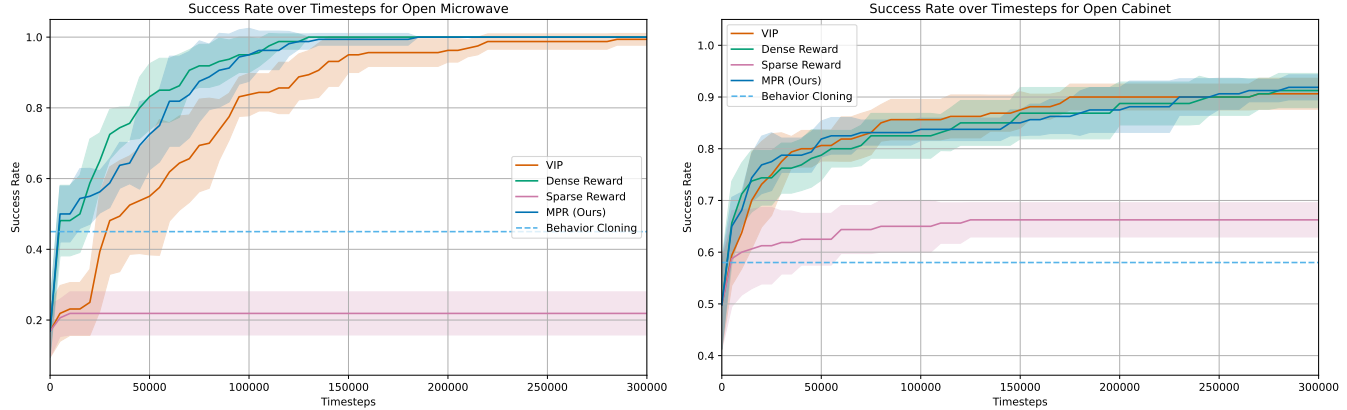


Fig. 2: **Success rates for various reward models across training timesteps in simulated tasks from the Franka Kitchen benchmark.** We evaluate different reward signals in our residual RL framework across two different simulated tasks. The reward signals include a sparse reward signal of 1 for task success and 0 otherwise, a handcrafted dense reward signal that measures progress to the goal using privileged simulation information, Value Implicit Pretraining (VIP) [34], which is representative of the temporal distance class of reward learning methods, and our work, Motion Prediction Reward (MPR). The success rates shown are calculated across 20 evaluations per checkpoint and 8 different seeds for each method. Standard deviations across the 8 seeds are shaded, and the dashed line shows the base policy performance. While both MPR and VIP match the handcrafted sparse reward in the cabinet task, MPR outperforms VIP in the microwave tasks and closely tracks the handcrafted reward performance.

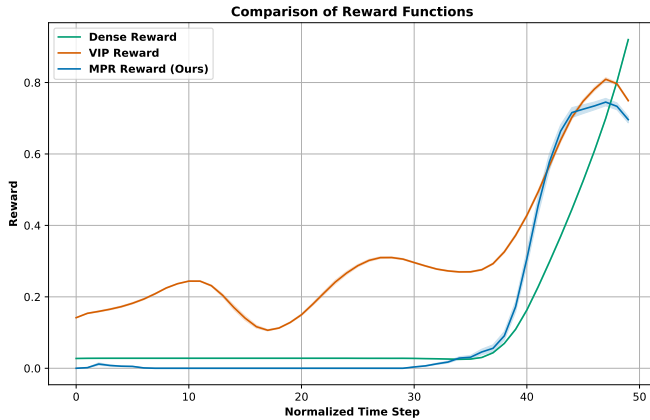


Fig. 3: **Comparison of reward signals across 50 successful demonstrations for the simulated “Open Microwave” task.** This plot shows the average estimated reward signal for our method (MPR), VIP [34], and a handcrafted dense reward signal that uses privileged simulation information. Our reward signal closely tracks the handcrafted reward and shows very little bias or false positive results.

estimation are taken from the world camera. We control the robot in the space of relative position deltas, where the action space is an 8-vector consisting of position, quaternion rotation, and gripper width. The observation space consists of the RGB images from the world camera and wrist cameras, the end-effector pose and gripper width, and the base policy action. We design a gymnasium[53]-like interface to parse actions from the robot policy and communicate observations back. For each task, we train the base diffusion policy with 10 teleoperated demonstrations. We then give the robot a budget

Method	Open Microwave	Fold Cloth	Wipe Counter
MPR (Ours)	$76.7 \pm 20.8\%$	$73.3 \pm 7.6\%$	$56.7 \pm 12.6\%$
VIP	$23.3 \pm 32.1\%$	$8.3 \pm 14.4\%$	$21.7 \pm 10.4\%$
Base Policy	45.0%	45.0%	40.0%

TABLE I: **Success rates for the three tasks on the robot hardware.** We evaluate the policies after 100 episodes of training in the real world. These success rates represent 20 evaluations of the final checkpoint across three different runs per method and task. The base policy performance is also shown to demonstrate the relative improvement.

of 100 episodes of environment interaction to improve using the given reward function with a critic and policy network updates after each episode. These 100 episodes take an hour to an hour and a half of wall clock time. We perform three runs for each reward function on each task, and the performance is evaluated on the final checkpoint across 20 episodes. Relative to the simulation experiments, we increase the update-to-data ratio to 4 (at the end of an episode, we perform four times as many gradient steps on the critic and policy networks as steps in the episode) to accelerate learning, and pretrain the critic network for 10,000 iterations using the demonstration data \mathcal{D} labeled with reward from each reward function. We also use a frozen pretrained DinoV2 encoder to process the image components of the state to accelerate learning. Even with these modifications, reinforcement learning on real robot hardware is very challenging as methods have a limited number of episodes and must learn in a very sample-efficient manner. Any bias or noise in a reward signal can significantly slow learning and limit the improvement the policy makes in the 100-episode window. Further details on the robot hardware setup are available in the Appendix in section IX.

Motion Prediction Reward outperforms VIP across all

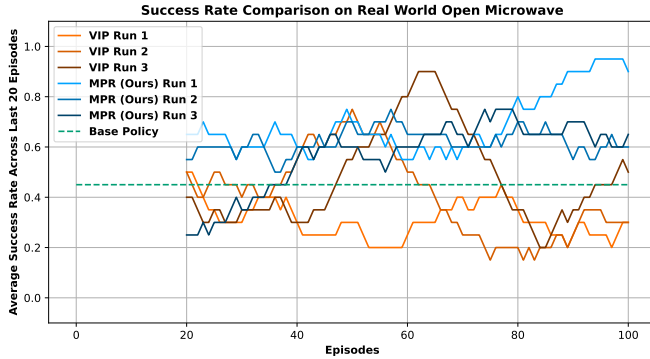


Fig. 4: **Real-world training performance for the “Open Microwave” task across three runs each for VIP [34] and our approach, Motion Prediction Reward (MPR).** All policies were initialized with the same base policy capable of completing the task 45% of the time (9/20 attempts) and trained for 100 episodes (about an hour of wall clock time). Our residual RL framework leveraged the demo data used to train the base policy (10 demonstrations) and data collected online, both labeled with reward signals generated by each method. The plot shows a running average success rate across the last 20 episodes, with VIP in shades of orange and MPR in shades of blue. All MPR runs improve over the base policy and finish with an average success rate of 76.7% across 20 evaluations on the final checkpoint. In contrast, the VIP runs face significant issues with stability and demonstrate “unlearning” behavior, finishing with an average success rate of 23.3%, well below the base policy’s performance.

hardware tasks. Table I shows the performance of the final checkpoints for each method across the three tasks, and Figure 4 shows the performance of each run for the “Open Microwave” task. Plots of training performance for the other two tasks, as well as further experiments, can be found in section XI in the Appendix. Across all three tasks, we observe that policies trained with our motion prediction reward outperform those trained with VIP. Compared to 300,000 training steps in simulation, on hardware, 100 episodes translate to about 15,000 steps. This greatly reduced training budget highlights that MPR reward signals lead to more sample-efficient learning than those estimated by VIP. In our hardware experiments, we observed certain cases where false positives from VIP led training to collapse. In the “fold cloth” task, the robot must reach for one corner of the cloth, grasp it, lift it, and bring it over to the other corner, and place it down to complete the fold. VIP rewards measure distances between the current and goal states. In this task the goal state was the robot with its end effector above the two stacked corners of the cloth at the end of the task. In one run, the VIP rewards led the robot to skip grabbing the first corner of the cloth, and move its end effector directly to the opposite corner and stop there. This indicates that the VIP reward function failed to capture the salient feature in this task, the folded cloth, and instead fixated on the robot’s position.

Motion Prediction Reward enables a robot to improve its own performance in real hardware trials. In the “Open Microwave” and “Fold Cloth” tasks, we observe an increase

in the success rate by 31.7 and 28.3 percentage points, respectively, over the base policies. In these tasks, with about an hour of training, MPR enables a robot to significantly increase its success rate while VIP is unable to match the performance of the base policy. In the “Wipe Counter” task, training with MPR rewards only yielded a 16.7% improvement over the base policy. During training on this task, we observed that the base policy trained with only 10 demos was very sensitive to the reset conditions, and its performance was inconsistent. This inconsistency also led to residual RL training with both reward models being particularly unstable on this task, highlighting the importance of the base policy in residual RL.

MPR reward estimation better discriminates between successful and failed episodes. Figure 4 shows the average success rates in a 20-episode sliding window for each of the three runs with MPR Reward (shades of blue) and VIP Reward (shades of orange) on the “Open Microwave”. Examining this plot, we see that while VIP has spans where its performance increases, its performance decreases just as quickly after, indicating the value function and policy learned with VIP rewards are demonstrating forgetting behavior. To understand why this happens to policies trained with VIP rewards, but not policies with MPR rewards, we plotted both reward functions and the learned value functions at the end of real-world training across a successful and a failed episode in Figure 5. As shown in Figure 5a, both reward models can recognize a successful episode, and the learned value functions reflect this quality. In the failed episode, the robot misses the handle of the microwave but still pulls back. While the robot goes through the motions of the task, the desired result, opening the microwave, is not actually achieved. MPR reward estimation does not give this episode any reward, as the task-relevant object, the microwave, never moved, and the value function learned by MPR clearly identifies that the robot has missed the handle and assigns a very low value to subsequent states. However, VIP reward estimation still assigns this failed episode some positive reward, and the learned value function does not recognize that the task has failed, or identify the point of failure. This can lead the learned value function to falsely assign positive value to failed episodes, and lead an actor attempting to maximize the value function to a local maxima, where the robot goes through the motions of the task and gets some reward, but doesn’t actually complete the task. We believe this property is the likely cause of the forgetting effect observed in training runs. As shown in the simulation results, more data mitigates this effect and enables the actor to find a more global maxima, but this makes policies learned with VIP reward less sample efficient, and reduces their efficacy in real-world training.

This result also indicates that MPR is likely capturing more salient features of the reward estimation process than VIP does. This is a benefit of MPR focusing on task-relevant objects, and a drawback of VIP having to transfer the estimated value function across a large distribution shift from human to robot videos. In addition, human video demonstrations primarily contain successful demonstrations. For this reason, methods that measure value as temporal distance may have a harder time distinguishing genuinely successful episodes from

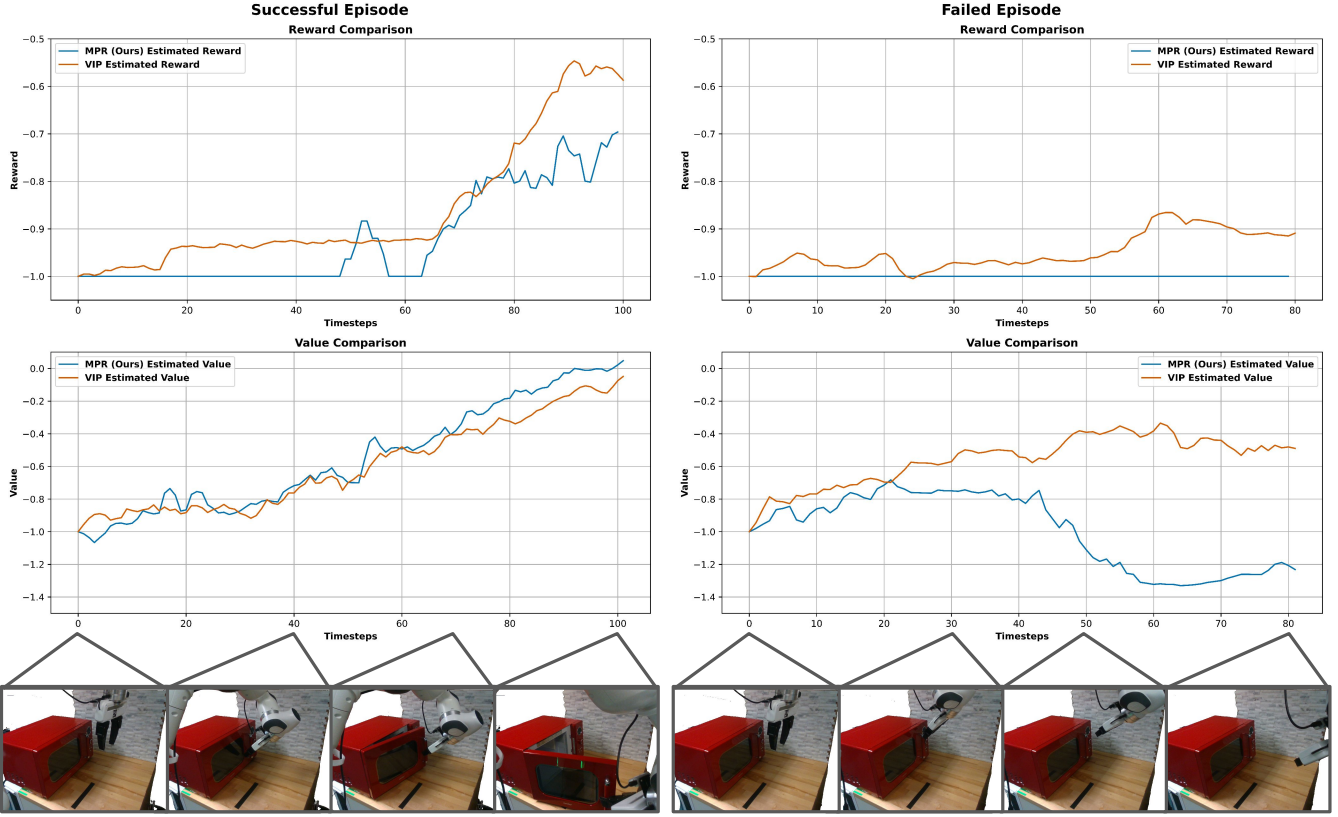


Fig. 5: **Estimated reward signals and value estimates after training from VIP and MPR show VIP has trouble identifying failed episodes.** Estimated rewards (top) and values computed by learned value functions (bottom) after 100 episodes of training by each reward model for a successful (left) and failed (right) episode. Note value estimates are computed using the full robot state (world image, wrist image, end-effector pose, and base action) and the policy’s action. Both approaches are capable of identifying a successful episode as shown in their reward and value estimates. However, VIP falsely assigns a moderate value to later actions and states in the failed episode, after the robot has missed grabbing the microwave handle, while MPR assigns no reward and a low value to the failed states.

episodes where the robot goes through the motions of the task but does not achieve success.

V. DISCUSSION

Our experiments show MPR significantly outperforms VIP across all tasks on real-hardware. However, VIP is a multitask policy conditioned via goal image, while MPR is trained for a specific task. In future work, we would like to explore a language-conditioned multi-task variant of MPR. Given the availability of human video data, and scaling in egocentric dataset size [1], we believe this work represents progress towards a dense reward foundation model for robot learning.

We explored a very low data scenario in this work, with only 10 demonstrations and an hour of policy refinement with the given reward function. While we saw promising results in our experiments, such limited data can be a challenge for reinforcement learning algorithms. Given the recent progress in video models and world models for robotics, we would like to explore search in a world model as another method for optimizing a policy to maximize our learned reward.

Finally, there are several ways we could continue to improve the quality of MPR models. We could finetune these models on

video from robot demonstrations, or collect in-domain human videos to adapt the motion prediction to the specific task. In developing this method, we also tested training our motion prediction models with diffusion rather than regression. While we saw more accurate motion prediction with the diffusion models, their inference time was significantly longer, and we felt the performance improvement didn’t justify the slower inference. We would like to revisit these models and experiment with ways to accelerate inference, potentially leveraging new flow-matching architectures.

VI. CONCLUSION

In this work, we demonstrated an approach to learning reward signals from human video by modeling per-step human preferences as the predicted motion of object points. This approach enabled us to transfer information from human video demonstrations of tasks to robots attempting to learn the same task. We demonstrated that with just 10 demonstrations and an hour of real-world training, our reward model enabled a robot to autonomously increase its performance on a task. We also observed that our approach to reward learning from human video significantly outperformed prior work that learned

temporal-distance based value functions. This work represents a promising new approach to reward learning from human video data, and we are excited to pursue it further.

ACKNOWLEDGMENTS

REFERENCES

- [1] Build AI. Egocentric-10k, 2025. URL <https://huggingface.co/datasets/builddotai/Egocentric-10K>.
- [2] Lars Ankile, Anthony Simeonov, Idan Shenfeld, Marcel Torne, and Pulkit Agrawal. From Imitation to Refinement – Residual RL for Precise Assembly, December 2024.
- [3] Lars Ankile, Zhenyu Jiang, Rocky Duan, Guanya Shi, Pieter Abbeel, and Anusha Nagabandi. Residual Off-Policy RL for Finetuning Behavior Cloning Policies, September 2025.
- [4] Mido Assran, Adrien Bardes, David Fan, Quentin Garido, Russell Howes, Mojtaba Komeili, Matthew Muckley, Ammar Rizvi, Claire Roberts, Koustuv Sinha, Artem Zholus, Sergio Arnaud, Abha Gejji, Ada Martin, Francois Robert Hogan, Daniel Dugas, Piotr Bojanowski, Vasil Khalidov, Patrick Labatut, Francisco Massa, Marc Szafrańiec, Kapil Krishnakumar, Yong Li, Xiaodong Ma, Sarath Chandar, Franziska Meier, Yann LeCun, Michael Rabbat, and Nicolas Ballas. V-JEPA 2: Self-Supervised Video Models Enable Understanding, Prediction and Planning, June 2025.
- [5] Arpit Bahety, Priyanka Mandikal, Ben Abbatematteo, and Roberto Martín-Martín. ScrewMimic: Bimanual Imitation from Human Videos with Screw Space Projection, May 2024.
- [6] Philip J. Ball, Laura Smith, Ilya Kostrikov, and Sergey Levine. Efficient Online Reinforcement Learning with Offline Data, May 2023.
- [7] Darrin C Bentivegna, Christopher G Atkeson, and Gordon Cheng. Learning From Observation and Practice Using Primitives.
- [8] Homanga Bharadhwaj, Roozbeh Mottaghi, Abhinav Gupta, and Shubham Tulsiani. Track2Act: Predicting Point Tracks from Internet Videos enables Generalizable Robot Manipulation, August 2024.
- [9] Ho Kei Cheng, Seoung Wug Oh, Brian Price, Joon-Young Lee, and Alexander Schwing. Putting the Object Back into Video Object Segmentation, April 2024.
- [10] Cheng Chi, Siyuan Feng, Yilun Du, Zhenjia Xu, Eric Cousineau, Benjamin Burchfiel, and Shuran Song. Diffusion Policy: Visuomotor Policy Learning via Action Diffusion, June 2023.
- [11] Cheng Chi, Zhenjia Xu, Chuer Pan, Eric Cousineau, Benjamin Burchfiel, Siyuan Feng, Russ Tedrake, and Shuran Song. Universal Manipulation Interface: In-The-Wild Robot Teaching Without In-The-Wild Robots, March 2024.
- [12] Dima Damen, Hazel Doughty, Giovanni Maria Farinella, Sanja Fidler, Antonino Furnari, Evangelos Kazakos, Davide Moltisanti, Jonathan Munro, Toby Perrett, Will Price, and Michael Wray. Scaling Egocentric Vision: The EPIC-KITCHENS Dataset, July 2018.
- [13] Dima Damen, Hazel Doughty, Giovanni Maria Farinella, Sanja Fidler, Antonino Furnari, Evangelos Kazakos, Davide Moltisanti, Jonathan Munro, Toby Perrett, Will Price, and Michael Wray. The EPIC-KITCHENS Dataset: Collection, Challenges and Baselines, April 2020.
- [14] Seyed Kamyar Seyed Ghasemipour, Ayzaan Wahid, Jonathan Tompson, Pannag Sanketi, and Igor Mordatch. Self-Improving Embodied Foundation Models, September 2025.
- [15] Kristen Grauman, Andrew Westbury, Eugene Byrne, Zachary Chavis, Antonino Furnari, Rohit Girdhar, Jackson Hamburger, Hao Jiang, Miao Liu, Xingyu Liu, Miguel Martin, Tushar Nagarajan, Ilija Radosavovic, Santhosh Kumar Ramakrishnan, Fiona Ryan, Jayant Sharma, Michael Wray, Mengmeng Xu, Eric Zhongcong Xu, Chen Zhao, Siddhant Bansal, Dhruv Batra, Vincent Cartillier, Sean Crane, Tien Do, Morrie Doulaty, Akshay Erapalli, Christoph Feichtenhofer, Adriano Fragnani, Qichen Fu, Abrham Gebreselasie, Cristina Gonzalez, James Hillis, Xuhua Huang, Yifei Huang, Wenqi Jia, Leslie Khoo, Jachym Kolar, Satwik Kottur, Anurag Kumar, Federico Landini, Chao Li, Yanghao Li, Zhenqiang Li, Karttikeya Mangalam, Raghava Modhugu, Jonathan Munro, Tullie Murrell, Takumi Nishiyasu, Will Price, Paola Ruiz Puentes, Merey Ramazanova, Leda Sari, Kiran Somasundaram, Audrey Southerland, Yusuke Sugano, Ruijie Tao, Minh Vo, Yuchen Wang, Xindi Wu, Takuma Yagi, Ziwei Zhao, Yunyi Zhu, Pablo Arbelaez, David Crandall, Dima Damen, Giovanni Maria Farinella, Christian Fuegen, Bernard Ghanem, Vamsi Krishna Ithapu, C. V. Jawahar, Hanbyul Joo, Kris Kitani, Haizhou Li, Richard Newcombe, Aude Oliva, Hyun Soo Park, James M. Rehg, Yoichi Sato, Jianbo Shi, Mike Zheng Shou, Antonio Torralba, Lorenzo Torresani, Mingfei Yan, and Jitendra Malik. Ego4D: Around the World in 3,000 Hours of Egocentric Video, March 2022.
- [16] Abhishek Gupta, Vikash Kumar, Corey Lynch, Sergey Levine, and Karol Hausman. Relay Policy Learning: Solving Long-Horizon Tasks via Imitation and Reinforcement Learning, October 2019.
- [17] Ritwik Gupta. Soft Actor Critic—Deep Reinforcement Learning with Real-World Robots. <http://bair.berkeley.edu/blog/2018/12/14/sac>.
- [18] Irmak Guzey, Yinlong Dai, Georgy Savva, Raunaq Bhairangi, and Lerrel Pinto. Bridging the Human to Robot Dexterity Gap through Object-Oriented Rewards, October 2024.
- [19] Nick Heppert, Max Argus, Tim Welschendorf, Thomas Brox, and Abhinav Valada. DITTO: Demonstration Imitation by Trajectory Transformation. In *2024 IEEE/RSJ International Conference on Intelligent Robots and Systems (IROS)*, pages 7565–7572, October 2024. doi: 10.1109/IROS58592.2024.10801982.
- [20] Hengyuan Hu, Suvir Mirchandani, and Dorsa Sadigh. Imitation Bootstrapped Reinforcement Learning, May 2024.
- [21] Arnav Kumar Jain, Vibhakar Mohta, Subin Kim, Atiksh

Bhardwaj, Juntao Ren, Yunhai Feng, Sanjiban Choudhury, and Gokul Swamy. A Smooth Sea Never Made a Skilled SAILOR: Robust Imitation via Learning to Search, October 2025.

[22] Nikita Karaev, Iurii Makarov, Jianyuan Wang, Natalia Neverova, Andrea Vedaldi, and Christian Rupprecht. Co-Tracker3: Simpler and Better Point Tracking by Pseudo-Labelling Real Videos, October 2024.

[23] Nikita Karaev, Ignacio Rocco, Benjamin Graham, Natalia Neverova, Andrea Vedaldi, and Christian Rupprecht. CoTracker: It is Better to Track Together, October 2024.

[24] Simar Kareer, Dhruv Patel, Ryan Punamiya, Pranay Mathur, Shuo Cheng, Chen Wang, Judy Hoffman, and Danfei Xu. EgoMimic: Scaling Imitation Learning via Egocentric Video, October 2024.

[25] Moo Jin Kim, Yihuai Gao, Tsung-Yi Lin, Yen-Chen Lin, Yunhao Ge, Grace Lam, Percy Liang, Shuran Song, Ming-Yu Liu, Chelsea Finn, and Jinwei Gu. Cosmos Policy: Fine-Tuning Video Models for Visuomotor Control and Planning, January 2026.

[26] Tony Lee, Andrew Wagenmaker, Karl Pertsch, Percy Liang, Sergey Levine, and Chelsea Finn. RoboReward: General-Purpose Vision-Language Reward Models for Robotics, January 2026.

[27] Marion Lepert, Jiaying Fang, and Jeannette Bohg. Masquerade: Learning from In-the-wild Human Videos using Data-Editing, August 2025.

[28] Jinhan Li, Yifeng Zhu, Yuqi Xie, Zhenyu Jiang, Mingyo Seo, Georgios Pavlakos, and Yuke Zhu. OKAMI: Teaching Humanoid Robots Manipulation Skills through Single Video Imitation, October 2024.

[29] Vincent Liu, Ademi Adeniji, Haotian Zhan, Siddhant Haldar, Raunaq Bhirangi, Pieter Abbeel, and Lerrel Pinto. EgoZero: Robot Learning from Smart Glasses, June 2025.

[30] Yuyang Liu, Chuan Wen, Yihang Hu, Dinesh Jayaraman, and Yang Gao. TimeRewarder: Learning Dense Reward from Passive Videos via Frame-wise Temporal Distance, September 2025.

[31] Jianlan Luo, Zheyuan Hu, Charles Xu, You Liang Tan, Jacob Berg, Archit Sharma, Stefan Schaal, Chelsea Finn, Abhishek Gupta, and Sergey Levine. SERL: A Software Suite for Sample-Efficient Robotic Reinforcement Learning, March 2025.

[32] Jianlan Luo, Charles Xu, Jeffrey Wu, and Sergey Levine. Precise and Dexterous Robotic Manipulation via Human-in-the-Loop Reinforcement Learning, March 2025.

[33] Yecheng Jason Ma, William Liang, Vaidehi Som, Vikash Kumar, Amy Zhang, Osbert Bastani, and Dinesh Jayaraman. LIV: Language-Image Representations and Rewards for Robotic Control, June 2023.

[34] Yecheng Jason Ma, Shagun Sodhani, Dinesh Jayaraman, Osbert Bastani, Vikash Kumar, and Amy Zhang. VIP: Towards Universal Visual Reward and Representation via Value-Implicit Pre-Training, March 2023.

[35] Parsa Mahmoudieh, Deepak Pathak, and Trevor Darrell. Zero-Shot Reward Specification via Grounded Natural Language. In *Proceedings of the 39th International Conference on Machine Learning*, pages 14743–14752. PMLR, June 2022.

[36] Arjun Majumdar, Karmesh Yadav, Sergio Arnaud, Yecheng Jason Ma, Claire Chen, Sneha Silwal, Aryan Jain, Vincent-Pierre Berges, Pieter Abbeel, Jitendra Malik, Dhruv Batra, Yixin Lin, Oleksandr Maksymets, Aravind Rajeswaran, and Franziska Meier. Where are we in the search for an Artificial Visual Cortex for Embodied Intelligence?, February 2024.

[37] Priyanka Mandikal, Jiaheng Hu, Shivin Dass, Sagnik Majumder, Roberto Martín-Martín, and Kristen Grauman. Mash, Spread, Slice! Learning to Manipulate Object States via Visual Spatial Progress, September 2025.

[38] Max Sobol Mark, Tian Gao, Georgia Gabriela Sampaio, Mohan Kumar Srirama, Archit Sharma, Chelsea Finn, and Aviral Kumar. Policy Agnostic RL: Offline RL and Online RL Fine-Tuning of Any Class and Backbone, December 2024.

[39] Lazar Milikic, Manthan Patel, and Jonas Frey. VLD: Visual Language Goal Distance for Reinforcement Learning Navigation, December 2025.

[40] Matthias Minderer, Alexey Gritsenko, and Neil Houlsby. Scaling Open-Vocabulary Object Detection, May 2024.

[41] Suraj Nair, Aravind Rajeswaran, Vikash Kumar, Chelsea Finn, and Abhinav Gupta. R3M: A Universal Visual Representation for Robot Manipulation, November 2022.

[42] Maxime Oquab, Timothée Darcet, Théo Moutakanni, Huy Vo, Marc Szafraniec, Vasil Khalidov, Pierre Fernandez, Daniel Haziza, Francisco Massa, Alaaeldin El-Nouby, Mahmoud Assran, Nicolas Ballas, Wojciech Galuba, Russell Howes, Po-Yao Huang, Shang-Wen Li, Ishan Misra, Michael Rabbat, Vasu Sharma, Gabriel Synnaeve, Hu Xu, Hervé Jegou, Julien Mairal, Patrick Labatut, Armand Joulin, and Piotr Bojanowski. DINOv2: Learning Robust Visual Features without Supervision, February 2024.

[43] Norman Di Palo and Edward Johns. DINOBot: Robot Manipulation via Retrieval and Alignment with Vision Foundation Models, February 2024.

[44] William Peebles and Saining Xie. Scalable Diffusion Models with Transformers, March 2023.

[45] Yuzhe Qin, Yueh-Hua Wu, Shaowei Liu, Hanwen Jiang, Ruihan Yang, Yang Fu, and Xiaolong Wang. DexMV: Imitation Learning for Dexterous Manipulation from Human Videos, July 2022.

[46] Nikhila Ravi, Valentin Gabeur, Yuan-Ting Hu, Ronghang Hu, Chaitanya Ryali, Tengyu Ma, Haitham Khedr, Roman Rädl, Chloe Rolland, Laura Gustafson, Eric Mintun, Junting Pan, Kalyan Vasudev Alwala, Nicolas Carion, Chao-Yuan Wu, Ross Girshick, Piotr Dollár, and Christoph Feichtenhofer. SAM 2: Segment Anything in Images and Videos, October 2024.

[47] Allen Z. Ren, Justin Lidard, Lars L. Ankile, Anthony Simeonov, Pulkit Agrawal, Anirudha Majumdar, Benjamin Burchfiel, Hongkai Dai, and Max Simchowitz. Diffusion Policy Policy Optimization, December 2024.

[48] Juntao Ren, Priya Sundaresan, Dorsa Sadigh, Sanjiban Choudhury, and Jeannette Bohg. Motion Tracks: A

Unified Representation for Human-Robot Transfer in Few-Shot Imitation Learning, October 2025.

- [49] Stephane Ross, Geoffrey J. Gordon, and J. Andrew Bagnell. A Reduction of Imitation Learning and Structured Prediction to No-Regret Online Learning, March 2011.
- [50] Pierre Sermanet, Corey Lynch, Yevgen Chebotar, Jasmine Hsu, Eric Jang, Stefan Schaal, and Sergey Levine. Time-Contrastive Networks: Self-Supervised Learning from Video, March 2018.
- [51] Lin Shao, Toki Migimatsu, Qiang Zhang, Karen Yang, and Jeannette Bohg. Concept2Robot: Learning Manipulation Concepts from Instructions and Human Demonstrations.
- [52] Yichao Shen, Fangyun Wei, Zhiying Du, Yaobo Liang, Yan Lu, Jiaolong Yang, Nanning Zheng, and Baining Guo. VideoVLA: Video Generators Can Be Generalizable Robot Manipulators, December 2025.
- [53] Mark Towers, Ariel Kwiatkowski, Jordan Terry, John U. Balis, Gianluca De Cola, Tristan Deleu, Manuel Goulão, Andreas Kallinteris, Markus Krimmel, Arjun KG, Rodrigo Perez-Vicente, Andrea Pierré, Sander Schulhoff, Jun Jet Tai, Hannah Tan, and Omar G. Younis. Gymnasium: A Standard Interface for Reinforcement Learning Environments, November 2025.
- [54] Yiqi Wang, Mrinal Verghese, and Jeff Schneider. Latent Policy Steering with Embodiment-Agnostic Pretrained World Models, September 2025.
- [55] Akihiko Yamaguchi, Christopher G. Atkeson, Scott Niekum, and Tsukasa Ogasawara. Learning pouring skills from demonstration and practice. In *2014 IEEE-RAS International Conference on Humanoid Robots*, pages 908–915, Madrid, Spain, November 2014. IEEE. ISBN 978-1-4799-7174-9. doi: 10.1109/HUMANOIDS.2014.7041472.
- [56] Zhecheng Yuan, Tianming Wei, Langzhe Gu, Pu Hua, Tianhai Liang, Yuanpei Chen, and Huazhe Xu. HERMES: Human-to-Robot Embodied Learning from Multi-Source Motion Data for Mobile Dexterous Manipulation, August 2025.
- [57] Yue Zhao, Ishan Misra, Philipp Krähenbühl, and Rohit Girdhar. Learning Video Representations from Large Language Models, December 2022.

This appendix is organized as follows:

7. Motion Prediction Model Training Details
8. Residual RL Details
9. Hardware Details
10. Behavior Cloning and RL Parameters
11. Additional Experimental Data

VII. MOTION PREDICTION MODEL TRAINING DETAILS

Our motion prediction model training pipeline includes the following steps

A. Task-Relevant Object Mask Tracking

We use OwlViT2 [40] to get the highest likelihood bounding box for a desired object and then prompt SAM2 [46] with this box to get an object mask. We run this detection for five frames equally sampled throughout the video and use the frame with the highest detection score. We then propagate this mask forward and backward in time using Cutie [9], a mask tracker. Using the estimated mask, we find a square 256x256 crop of the video such that the task-relevant object is always visible. If needed, we crop a larger square and then downsample to 256x256 to ensure the task-relevant objects are visible throughout the whole video.

B. Point Tracking

We use CoTracker3 [22] to track an evenly sampled grid of 32x32 points in the video. CoTracker provides point locations and estimated visibility. We keep track of the proportion of visible points on the task-relevant objects, and if more than 30% of them become no longer visible, we resample the grid of points. This helps account for cases where an object moves or the camera perspective shifts, causing us to lose track of points. We observed that CoTracker’s performance decreases with very short horizon tracks, so we set a threshold of 30% to balance good point density with minimal point resamples. We construct our training dataset where the inputs are the current and previous frames from the video, the point locations in the current frame, and the current frame number divided by the total length of the video, and the targets are the point locations in the next frame. We use an input of two frames to give the model context for any existing motion. We remove any frames from the training data where the max point motion is below 0.5 pixels, to avoid cases where frames are duplicated or there is no motion. We also normalize the point locations to be between zero and one.

C. Input Preparation

Using the masks of each frame and the point locations, we designate points in the mask as object points and points outside the mask as background points. We calculate the average vector of background point motion and subtract it from the object point motion. This helps compensate for the camera motion in egocentric video. At each frame, we use all object points and sample half the number of object points from the set of background points. This focuses learning on object point prediction, but still requires the network to compensate for any residual background motion. During initial testing, we found this mixture to be more effective than sampling all points or only object points. To make uniform batches during

training, we repeat this set of points until we hit 300 points. We preprocess frames with the standard ImageNet normalization.

D. Training parameters

Parameter	Value
Epochs	1000
Batch Size	20
Learning Rate	$1e^{-4}$
Val Ratio	0.1
Optimizer	AdamW
Architecture	DiT
# Params	560M

TABLE II: Motion Prediction Transformer training parameters.

E. Inference

We use the same input preparation process during inference, with the exception that we don’t subtract background point motion, as our camera is fixed during inference. Our reward function computes a reward value between zero and one. During testing, we found that with a positive reward, the robot would become disinclined to complete the task, as completing the task ended the episode. Instead, it would keep manipulating task-relevant objects to try to get more positive rewards. To discourage this behavior, we just subtracted one from the reward output to shift the range to negative one to zero.

F. Hardware

All training was done on two RTX 4090s with 24GB of VRAM each. Training takes 12-48 hours, depending on the number of videos in the training set. Inference was done using one 4090, with the mask tracking stack and CoTracker running on the other 4090. Inference with full masking, tracking, and computation takes 5-10 seconds per episode.

VIII. RESIDUAL RL DETAILS

We implement our residual RL framework as a modified version of Soft Actor Critic (SAC) [17]. We primarily follow the modifications outlined in RLPD from Ball et al. [6] and apply them to the implementation of SAC in Stable Baselines 3 (SB3). SB3 already includes training dual critic networks and taking a minimum across critics for value estimation. Additionally, we add LayerNorm after all but the last layers of the critic network. We find that this has a significant impact on learning stability. Following RLPD, we sample evenly from the offline buffer containing the demonstration data and the online buffer containing collected transitions. Following Ankile et al. [2], we apply orthogonal initialization to actor weights with 0 bias. Full RL parameters can be found in Section X of this appendix.

For efficiency and smooth execution on hardware, we perform reward computation and training at the end of each episode. We write a Gym wrapper to cache images from execution, and an SB3 callback to run after episode collection and compute reward signals.

IX. HARDWARE DETAILS

We use a Franka Research 3 robot for all hardware experiments. This robot is equipped with two RealSense D435 cameras, one in a fixed “over-the-shoulder” location and one attached to the wrist joint. The robot is equipped with a parallel jaw gripper and has its provided fingers replaced with compliant UMI fingers [11]. We use the Polymetis library to control our Franka robot. Polymetis leverages a separate control PC with a real-time kernel patch running a low-level controller at a higher frequency, and then an inference PC running a learned controller at a lower frequency. We run impedance control for both data collection and inference. This impedance controller runs at approximately 1000Hz on the control PC and provides high responsiveness while also preventing the robot from damaging itself or the environment. The impedance controller also lets the robot modulate force by adjusting its set point. We run our learned policy at approximately 10 Hz. During RL training and inference, we apply an additional damping factor of 0.1 on the magnitude of all commanded rotations. High-magnitude rotation commands can cause errors in the controller, and we found that rotation was particularly affected by action noise during training. This would add significant noise to the position of the end-effector and slow training. Additionally, total rotation commands are clipped to have a magnitude no greater than 0.25 radians.

X. BEHAVIOR CLONING AND RL PARAMETERS

A. Behavior Cloning Parameters

Parameter	Value
Epochs	1000
Batch Size	64
Learning Rate	$1e^{-4}$
Architecture	Conditional UNet 1D
UNet Parameters	94.8M
Optimizer	AdamW
Optimizer Weight Decay	$1e^{-6}$
Optimizer Betas	0.9, 0.95
LR Schedule	Cosine
Diffusion Steps	50
Diffusion Scheduler	DDPM
Diffusion Beta Start	$1e^{-4}$
Diffusion Beta End	$2e^{-2}$
Diffusion Beta Schedule	Squared Cosine
Vision Encoder	ResNet18
Vision Encoder Parameters	11.7M
EMA Model Power	0.75
Observation Horizon	2
Prediction Horizon	16
Action Horizon	8

TABLE III: Diffusion Policy Behavior Cloning Parameters.

B. RL Parameters

Note, we only include parameters here that are different than their default values. To find a full list of SAC parameters, see the Stable Baselines 3 documentation.

XI. ADDITIONAL EXPERIMENTAL DATA

A. Run Visualization for Fold Cloth and Wipe Counter

We include here the average success rates across the last 20 episodes for each of the three runs of each method in the

Parameter	Value
Batch Size	64
Learning Rate	$1e^{-4}$
γ	0.99
Offline Ratio	0.5
Learning Starts	1024
Update to Data Ratio	4
Train Frequency	Every Episode
Network Hidden Size	256
Network Hidden Layers	3
Vision Encoder	Frozen DinoV2 ViT Small

TABLE IV: Soft Actor Critic Parameters.

“Fold Cloth” and “Wipe Counter” tasks. Training runs in the “Wipe Counter” task are less stable due to the base policy training on 10 demos being sensitive to reset conditions.

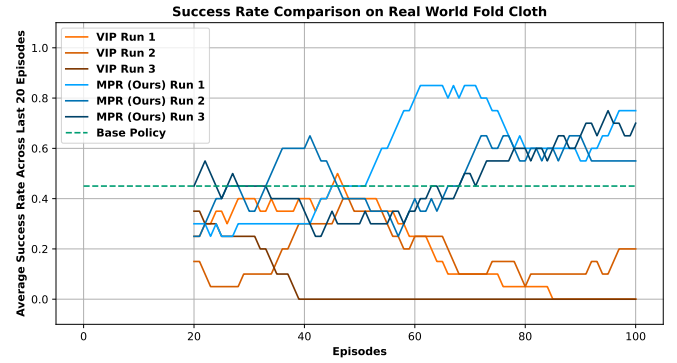


Fig. 6: Real-world training performance for the “Fold Cloth” task across three runs each for VIP [34] and our approach, Motion Prediction Reward (MPR). All policies were initialized with the same base policy capable of completing the task 45% of the time (9/20 attempts) and trained for 100 episodes (about an hour of wall clock time).

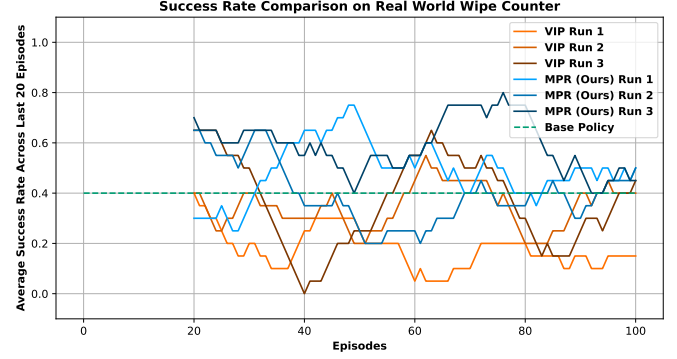


Fig. 7: Real-world training performance for the “Wipe Counter” task across three runs each for VIP [34] and our approach, Motion Prediction Reward (MPR). All policies were initialized with the same base policy capable of completing the task 40% of the time (8/20 attempts) and trained for 100 episodes (about an hour of wall clock time).

B. Ablation on Object Masking

We test the effects of removing the object-masking component from our training and inference pipelines. Instead of

training to predict task-relevant object motion, we predict the motion of every point in the scene. This also removes our ability to subtract background motion from point tracks to compensate for camera motion in egocentric video. During training, this model exhibits overfitting behavior as evidenced by a rise in validation loss, which we didn't observe when training models with object masking. Figure 8 shows the reward signal on the open microwave task for this ablated version of the model, and Figure 9 shows the learning performance during training. Without object masking, the learned reward signal is significantly noisier and results in less sample-efficient learning in the simulated task.

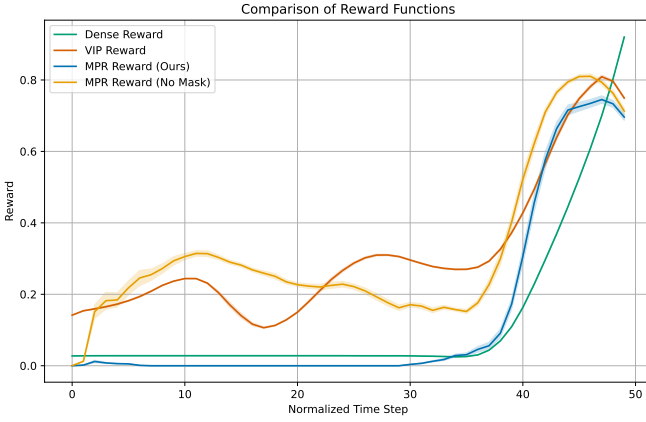


Fig. 8: **Comparison of reward signals across 50 successful demonstrations for the simulated “Open Microwave” task.** This plot includes an ablated version of our method that doesn't use task-relevant object masking.

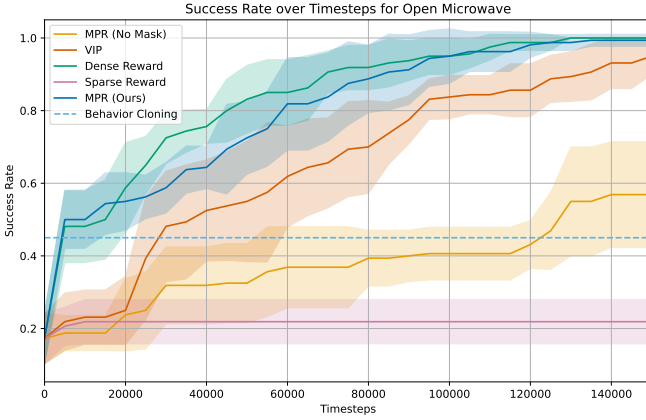


Fig. 9: **Success rates for an ablated version of our Motion Prediction Reward without object masking evaluated on the open microwave task from the Franka Kitchen benchmark [16].** The ablated version is less sample efficient.

C. Comparison to RoboReward

We also evaluate our approach against RoboReward [26], a robot reward foundation model. RoboReward is a Qwen3-VL 8 billion parameter model that has been finetuned on the Open X-Embodiment dataset annotated with reward values. RoboReward takes as input a video of task execution and the

task language description, and outputs a sparse reward signal from 1-5 that rates the robot's performance on the task. While RoboReward outperforms the sparse reward signal provided by the environment (one for task success and zero otherwise), it underperforms all other methods that provide dense, per-step rewards.

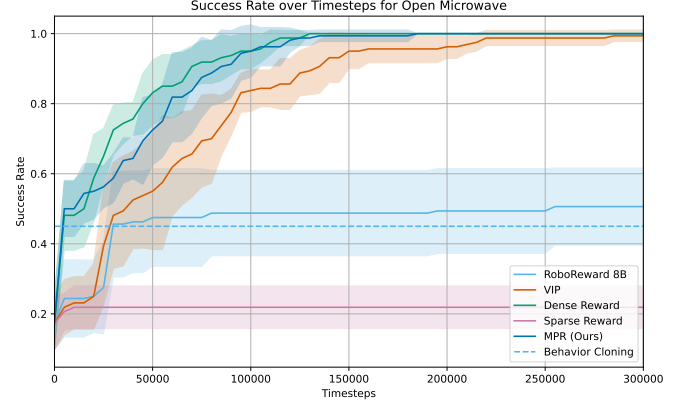


Fig. 10: **Success rates including results with the RoboReward [26] 8 billion parameter model on the open microwave task from the Franka Kitchen benchmark [16].**

D. Task Visualization

Figure 11 shows a visualization of the three tasks we tested on hardware.



Fig. 11: Visualization of the three different skills tested on hardware: “Open Microwave”, “Fold Cloth”, and ”Wipe Counter”.